

Partial Lattice Defects in Higher-Order Topological Insulators

Raquel Queiroz,^{1,*} Ion Cosma Fulga,^{2,†} Nurit Avraham,¹ Haim Beidenkopf,¹ and Jennifer Cano^{3,4,5,‡}

¹*Department of Condensed Matter Physics, Weizmann Institute of Science, Rehovot 7610001, Israel*

²*Institute for Theoretical Solid State Physics, IFW Dresden, Helmholtzstr. 20, 01069 Dresden, Germany*

³*Princeton Center for Theoretical Science, Princeton University, Princeton, New Jersey 08544, USA*

⁴*Department of Physics and Astronomy, Stony Brook University, Stony Brook, New York 11974, USA*

⁵*Center for Computational Quantum Physics, Flatiron Institute, New York, New York 10010, USA*



(Received 18 September 2018; revised manuscript received 28 February 2019; published 27 December 2019)

Nonzero weak topological indices are thought to be a necessary condition to bind a single helical mode to lattice dislocations. In this work we show that higher-order topological insulators (HOTIs) can, in fact, host a single helical mode along screw or edge dislocations (including step edges) in the absence of weak topological indices. When this occurs, the helical mode is necessarily bound to a dislocation characterized by a fractional Burgers vector, macroscopically detected by the existence of a stacking fault. The robustness of a helical mode on a partial defect is demonstrated by an adiabatic transformation that restores translation symmetry in the stacking fault. We present two examples of HOTIs, one intrinsic and one extrinsic, that show helical modes at partial dislocations. Since partial defects and stacking faults are commonplace in bulk crystals, the existence of such helical modes can measurably affect the expected conductivity in these materials.

DOI: [10.1103/PhysRevLett.123.266802](https://doi.org/10.1103/PhysRevLett.123.266802)

Introduction.—Topological insulators (TI) with weak indices [1–3] have the distinctive property of hosting single one-dimensional (1D) helical modes on line dislocations [4–6]. These topological modes can be regarded as more robust than the helical surface states of a weak topological insulator (WTI) because they do not require translation symmetry for protection [4,5,7]. Thus, they are a valuable tool to identify and probe the physics of WTIs experimentally [8–10]. Beyond WTIs, the existence of protected gapless modes localized on topological defects generalizes to band insulators in other dimensions and symmetry classes [5,11–15], as well as to topological band insulators protected by crystal symmetry [16–22].

Partial dislocations—those whose Burgers vector is a fraction of a lattice translation—fall outside of the topological classification: because partial dislocations are necessarily accompanied by a stacking fault plane, they are locally detectable arbitrarily far away from the dislocation line and, thus, do not constitute a topological defect. However, as we show in the Letter, partial dislocations can host topologically protected gapless modes. Since multiple partial dislocations can combine to form a full dislocation, consistency with the classification in Ref. [5] provides conditions under which a partial dislocation can exhibit a gapless topological mode.

We find that the existence of topological modes on partial defects is intimately related to the recently predicted higher-order topological insulators (HOTIs) [23–40]. HOTIs of order d in D spatial dimensions are characterized by gapless topological modes on their $D - d$ dimensional

edges. These gapless modes reside between $(D - d + 1)$ -dimensional surfaces that are gapped by mass terms of different sign. If the mass term on either side of the $(D - d)$ -dimensional edge is forced to differ in sign because the corresponding $(D - d + 1)$ -dimensional surfaces are related by symmetry, then the HOTI is *intrinsic*: its topological edge mode cannot be removed without closing the bulk gap or breaking crystal symmetry. In contrast, the gapless $(D - d)$ -dimensional edge modes of *extrinsic* HOTIs can be removed while preserving the bulk gap and crystal symmetry, by closing the surface gap [28]. HOTIs, like WTIs and topological crystalline insulators [41,42], have a trivial bulk in the absence of crystal symmetries.

In this Letter, we focus on $D = 3$, $d = 2$. We prove that a system whose partial dislocations host a gapless topological 1D mode must either have gapless surface states or realize an intrinsic or extrinsic HOTI for some surface termination. Focusing on symmetry class AII [43]—although our results can be generalized—we present two models of an intrinsic and an extrinsic second order topological insulator, which have trivial weak indices, but which realize gapless helical modes on partial screw dislocations. Both models can be smoothly deformed to a WTI by symmetrizing the Hamiltonian such that the unit cell is halved. During this process, the bulk gap remain open, while the surface gap closes; thus, the deformation of the Hamiltonian is accompanied by an insulator-to-metal surface phase transition. The existence of a partial Burgers vector in a HOTI that can be elevated to a full lattice vector

in a WTI without closing the bulk gap is a sufficient condition to realize a helical mode on a partial dislocation. More generally, we prove that a gapless helical mode on a partial lattice dislocation is an unambiguous signature of topology and that, in the reverse direction, for every HOTI with gapless helical modes on its hinges, there exists a lattice defect that exhibits a gapless helical mode.

The existence of helical modes bound to defects is a valuable probe to experimentally detect HOTIs in cases where the $(D - d)$ -dimensional (hinge) modes are not visible.

Partial screw and edge dislocations.—A dislocation line is characterized by a lattice vector \mathbf{B} , the Burgers vector. The dislocation breaks lattice translation symmetry, but away from the line, translation symmetry is restored, rendering the line dislocation locally invisible. Hence, a line dislocation is a *topological* defect because it is only detectable by a nonlocal probe: a loop around the line dislocation can only be closed with an additional translation of \mathbf{B} relative to the same loop without the defect. When a dislocation terminates at a surface, it results in a step edge, depicted in Fig. 1.

Edge and screw dislocations are distinguished by whether \mathbf{B} is perpendicular or parallel to the defect, respectively. A general dislocation can be a combination.

In a crystalline system, topological defects are classified by how the Bloch Hamiltonian winds as it is transported around the defect [5]. In three-dimensional time-reversal invariant systems with spin-orbit coupling (class AII), a line defect is classified by a \mathbb{Z}_2 invariant, which indicates

whether it hosts a helical mode [5]. The \mathbb{Z}_2 invariant corresponding to a dislocation described by \mathbf{B} is determined completely by the weak indices of the Hamiltonian [4]: it is nontrivial if

$$\mathbf{B} \cdot \mathbf{M}_\nu = \pi \pmod{2\pi}, \quad (1)$$

where the time-reversal invariant momentum $\mathbf{M}_\nu = (\nu_1 \mathbf{G}_1 + \nu_2 \mathbf{G}_2 + \nu_3 \mathbf{G}_3)/2$ is determined by the weak topological indices (ν_1, ν_2, ν_3) and the reciprocal lattice vectors \mathbf{G}_i [1–3].

Here, we consider topological helical modes at dislocations that are characterized by a Burgers vector that is *not* a lattice vector, which we denote by \mathbf{b} . Such a defect is referred to as a *partial* dislocation [44]. A partial dislocation is always bound to a stacking fault—a 2D plane where translation symmetry is broken—as shown in Fig. 1. Thus, a partial dislocation is not a topological defect and, consequently, Eq. (1) does not apply. In fact, we will show that a system with trivial weak indices can host a single gapless helical mode on a partial dislocation.

To gain insight into which partial dislocations can host helical modes, we derive a general constraint by combining multiple partials to form a full dislocation: suppose \mathbf{b} characterizes a partial dislocation that hosts h gapless helical modes, and define $n > 1$ be the minimum integer such that $n\mathbf{b}$ is a lattice vector. (The case $n = 2$ is depicted in Fig. 1.) Then consider the full dislocation characterized by $n\mathbf{b}$. This dislocation hosts $nh \pmod{2}$ helical modes. Comparison with Eq. (1) requires

$$n\mathbf{b} \cdot \mathbf{M}_\nu = nh\pi \pmod{2\pi}. \quad (2)$$

There are four cases: First, if n is even and $n\mathbf{b} \cdot \mathbf{M}_\nu = 0$, then any value of h satisfies Eq. (2); in particular, a system may have trivial weak indices and yet host gapless helical modes on partial defects. This is the case considered in the models that follow. Second, if n is even and $n\mathbf{b} \cdot \mathbf{M}_\nu = \pi$, then there is no $h \in \mathbb{Z}$ that satisfies Eq. (2); hence, the stacking fault that accompanies \mathbf{b} must be gapless. Third, if n is odd and $n\mathbf{b} \cdot \mathbf{M}_\nu = \pi$, then h must be odd and hence the partial screw dislocation *must* host a gapless helical mode if the stacking fault is gapped. Finally, if n is odd and $n\mathbf{b} \cdot \mathbf{M}_\nu = 0$, then h must be even: the partial defect *cannot* host a single gapless helical mode. A look-up table summarizes these results in the Supplemental Material, Sec. A [45].

Connection to HOTIs.—We now argue that a system that realizes a helical mode on a partial dislocation is an (extrinsic or intrinsic) HOTI or has gapless surface states. This follows because a step edge can be deformed into a “hinge” between two surfaces of a crystal, depicted in Fig. 1(c) and shown numerically in the Supplemental Material, Sec. B [45]. Specifically, if a helical mode exists on a partial dislocation, then the same mode must exist on a partial step edge where the dislocation terminates on a

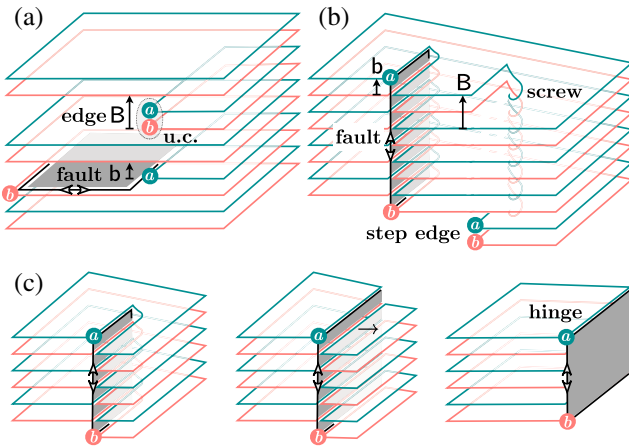


FIG. 1. Full and partial dislocations with Burgers vectors \mathbf{B} and \mathbf{b} , respectively; a and b indicate sublattice degrees of freedom in the unit cell. \mathbf{B} is a lattice translation, while \mathbf{b} is not. The dislocations are either (a) edge dislocations or (b) screw dislocations. A full dislocation is locally invisible away from its core. In contrast, a partial dislocation is attached to a 2D stacking fault (gray plane). This partial dislocation can host a helical mode, indicated by a black line and double arrow. (c) Adiabatic deformation of the lattice, taking the stacking fault into the surface. The helical mode localized at a screw dislocation mode can be moved into the hinge.

surface. The partial step edge can be turned into a hinge by adding or removing atoms until it reaches the edge of the crystal. Because the topological protection of the helical mode only depends on time-reversal symmetry, it will be robust to this deformation provided it does not encounter another gapless mode, either on the hinge (in which case the material is already a HOTI) or on the side surface. Thus, this construction yields a surface termination with a gapless helical mode; hence, it is a HOTI. However, the existence of the helical mode on a partial dislocation does not depend on the surface termination; it is a bulk characteristic.

In the reverse direction, given a HOTI with gapped surfaces (which excludes a WTI) and gapless helical modes on its hinges, a defect with a gapless helical mode can be engineered by “stacking” in real space multiple copies so that an external hinge mode becomes an internal defect and translation is broken across the stacking plane. Depending on the spatial embedding of the degrees of freedom in the HOTI, this defect may be a partial dislocation; it cannot be a full dislocation (otherwise, it would be a WTI). If the Hamiltonian can be smoothly deformed to preserve translation symmetry across the stacking plane, then the defect was necessarily a partial dislocation and the deformed system is a WTI with a helical mode on a full dislocation.

Models.—We present two models of 3D HOTIs, characterized by a gapped bulk and gapped surfaces, but gapless helical modes along one-dimensional edges. They are both “doubled” models, constructed from two interpenetrating sublattices that separately realize a topological phase (either a weak or strong TI), but combined the system has trivial weak and strong indices. Both models can be continuously deformed to a WTI without closing the bulk gap by turning off the intersublattice coupling, which halves the unit cell. When the sublattices are coupled, they have trivial weak (and strong) indices, but nonetheless host gapless helical modes on certain partial screw dislocations. In Supplemental Material, Sec. C [45], we prove that the helical modes are required by computing the nontrivial \mathbb{Z}_2 invariant of the stacking fault.

Extrinsic HOTI.—We start with a WTI constructed from 2D quantum spin Hall (QSH) layers stacked evenly with spacing \hat{z} . We add a perturbation that alternates the coupling between adjacent layers, doubling the unit cell without closing the bulk gap; this is a generalization of the Su-Schrieffer-Heeger chain [49]. Terminating the system between strongly coupled layers will reveal 1D helical modes along its hinges, while terminating between weakly coupled layers yields gapped hinges. This model comprises an *extrinsic* HOTI [28], since the presence or absence of helical hinge modes depends on the surface termination. Consequently, the extrinsic HOTI is not symmetry indicated [20,50]: the quantum numbers associated with wave functions at high-symmetry points in the Brillouin zone do not yield a bulk topological invariant.

We consider the first quantized Hamiltonian $H(\mathbf{k}) = H_0(\mathbf{k})\mu_0 + H_\delta(\mathbf{k})$, where \mathbf{k} labels the crystal momentum, σ_z and τ_z the spin and orbital degrees of freedom, and μ_z a sublattice index labeling the two inequivalent sites in the dimerized unit cell. We define

$$H_0(\mathbf{k}) = M(\mathbf{k})\tau_z - A(\sin k_x\sigma_x - \sin k_y\sigma_y)\tau_x, \quad (3)$$

with $M(\mathbf{k}) = M - B(4 - 2\cos k_x - 2\cos k_y)$ and $0 < M < 4B$, which describes a 2D TI in each layer, and

$$H_\delta(k_z) = [(t - \delta)\mu_y - (t + \delta)(\cos k_z\mu_y - \sin k_z\mu_x)]\sigma_z\tau_x, \quad (4)$$

which couples the layers in a dimerized fashion. When $\delta = 0$, H describes a WTI with indices (0;001) and a lattice translation of \hat{z} . Away from this fine-tuned point, when $\delta \neq 0$, but δ is much smaller than the bulk gap, the system remains adiabatically connected to a WTI, but its unit cell is doubled and, consequently, its \mathbb{Z}_2 indices are trivial, (0;000). The new cell causes the Brillouin zone to fold; hence, when $\delta \neq 0$, the gapless surfaces of the WTI (at $\delta = 0$) become gapped. Furthermore, when $\delta \neq 0$, the system can be terminated such that two gapless helical modes reside along its top and bottom edges [Fig. 2(a)]; thus, it is an extrinsic HOTI.

When $\delta = 0$, a screw dislocation that connects two adjacent layers ($\mathbf{B} = \hat{z}$) is a full dislocation that hosts a helical mode according to Eq. (1). When $\delta \neq 0$, the helical mode remains (its topological protection does not rely on translation symmetry), but since \hat{z} is not a lattice vector, the dislocation is partial. Hence, this model has trivial weak indices and a helical mode along a partial dislocation.

Using the Kwant code [51], we have numerically implemented this model on a finite size sample of 20^3 sites, setting $M = 2$, $A = B = 1$, $t = 0.3$, and $\delta = 0.2$. Figure 2(a) shows the helical modes on the top and bottom surfaces. Figure 2(b) shows the partial screw dislocation with $\mathbf{b} = \hat{z}$, confirming that the gapless helical mode is bound to the dislocation core as well as to step edges that emanate from it. (See Supplemental Material, Sec. D [45]

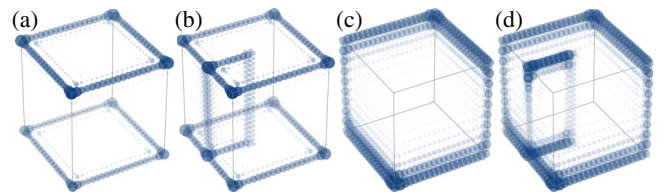


FIG. 2. HOTIs with screw dislocations. (a) Hinge modes of the extrinsic HOTI [Eqs. (3) and (4)]. (b) The extrinsic HOTI with a single partial screw dislocation. (c) Hinge modes of the intrinsic inversion-protected HOTI [Eqs. (5) and (6)]. (d) The intrinsic HOTI with a single partial screw dislocation. In all panels, the real-space probability distribution is averaged over the eight states closest to $E = 0$. Larger circles and darker colors correspond to larger probability densities.

for band structure.) Our numerical simulation shows a surface termination realizing the extrinsic HOTI phase. However, since the helical mode is a bulk feature, it will reside on the screw dislocation regardless of the surface termination.

Intrinsic HOTI.—Our second model consists of two coupled strong 3D TIs, one on each of the two sublattices (labeled a and b). Each 3D TI is described by

$$H_0(\mathbf{k}) = M(\mathbf{k})\tau_z + A(\sin k_x\sigma_z\tau_x - \sin k_y\tau_y + \sin k_z\sigma_x\tau_x), \quad (5)$$

where $M(\mathbf{k}) = M - B(6 - 2\cos k_x - 2\cos k_y - 2\cos k_z)$. $H_0(\mathbf{k})$ obeys time-reversal symmetry, $\mathcal{T} = i\sigma_y K$, where K is complex conjugation, and inversion symmetry, $\mathcal{P} = \tau_z$. We consider the regime $0 < M < 4B$, where there is one occupied Kramers pair (at Γ) with negative inversion eigenvalues.

We now introduce a sublattice degree of freedom, indexed by μ_z . The Hamiltonian $H_0(\mathbf{k})\mu_0$ describes two (uncoupled) 3D TIs. This model was introduced as the “double strong TI” (DSTI) [31], without specifying the spatial embedding of the sublattices. Here, we offset the b sublattice half a unit cell in the \hat{z} direction. This shift preserves the inversion center about the origin. It also introduces a translation symmetry by $\hat{z}/2$, denoted $\mathbf{t}_{z/2}$, which exchanges the two sublattices. The extra translation symmetry causes the Brillouin zone to unfold so that the two band inversions are now located at Γ and $Z \equiv (0, 0, \pi)$. Consequently, $H_0(\mathbf{k})\mu_0$ describes a WTI with indices $(0; 001)$.

We add a perturbation that breaks $\mathbf{t}_{z/2}$ down to \mathbf{t}_z and gaps all surfaces:

$$H_\delta(\mathbf{k}) = m \sin \frac{k_z}{2} \sigma_y \tau_x \mu_x + \delta \cos \frac{k_z}{2} (\sigma_x \tau_z + \sigma_y \tau_0) \mu_y. \quad (6)$$

The first term preserves $\mathbf{t}_{z/2}$ symmetry, but gaps the surface Dirac cones (one from each sublattice) on the \hat{z} -normal surface. The second term breaks $\mathbf{t}_{z/2}$ symmetry and thus gaps the Dirac cones on the \hat{x} - and \hat{y} -normal surfaces; in an electronic system, this can emerge from a charge density wave or a Jahn-Teller distortion. Thus, $H(\mathbf{k}) = H_0(\mathbf{k})\mu_0 + H_\delta(\mathbf{k})$ has a gapped bulk and surfaces. Its \mathbb{Z}_2 indices are trivial, $(0; 000)$. However, the inversion eigenvalues of the occupied bands yield a nontrivial HOTI index of $2 \bmod 4$ [31]. This model realizes an *intrinsic* HOTI: a finite sample realizes a single helical mode that cannot be removed without breaking inversion symmetry. (If inversion symmetry is broken, the helical mode will persist provided all bulk and surface gaps remain open.)

We now insert partial screw dislocation with $\mathbf{b} = \hat{z}/2$. When $m = \delta = 0$ and $\mathbf{t}_{z/2}$ symmetry is preserved, this is a full dislocation that hosts a single helical mode according to Eq. (1). When $m, \delta \neq 0$, the dislocation is partial, but as

long as $H_\delta(\mathbf{k})$ does not close the bulk gap, the helical mode must survive. Thus, we have provided an example of an intrinsic HOTI in which a partial screw dislocation hosts a gapless helical mode, while the bulk has trivial \mathbb{Z}_2 indices.

We numerically implemented this model on a finite size sample of $20 \times 20 \times 19$ sites, with $M = 2$, $A = B = 1$, $m = 2$, and $\delta = 0.5$. Figure 2(c) shows the single helical mode that traverses an inversion-symmetric path across the hinges. Figure 2(d) shows the partial screw dislocation with $\mathbf{b} = \hat{z}/2$, which hosts a gapless helical mode along the dislocation as well as on the step edges on the top and bottom surfaces. (See Supplemental Material, Sec. D [45] for band structure.)

Edge dislocations.—Because screw and edge dislocations can be deformed into each other, edge dislocations in HOTIs can also realize gapless helical modes, which we demonstrate in the Supplemental Material, Sec. E [45].

Measurement.—Partial lattice defects are ubiquitous in crystals [44]. Their presence can be detected by a surface step edge, whose height reveals whether it is partial or full. The density of states on the step edge can be measured via scanning tunneling spectroscopy (STS), as has been demonstrated for several topological materials [30,52–61].

Recently, $1T'$ -MoTe₂ and $1T'$ -WTe₂ were predicted to be intrinsic HOTIs [62]. The latter is unstable in bulk form; however, STS reveals topological edge modes on single-layer $1T'$ -WTe₂ [58,59]. Since the bulk unit cell contains two such layers, a single-layer step edge is a partial dislocation; thus, the measurement is consistent with our analysis. While bismuth [30] and SnTe [24] have also been predicted to be intrinsic HOTIs and zero bias peaks have been measured on full step edges in both materials [30,52,54], they fall outside of the scope of our work because neither can be adiabatically connected to a WTI.

We propose a candidate *extrinsic* HOTI, Bi₁₃Pt₃I₇, which consists of dimerized 2D TI layers [53], similar to the extrinsic HOTI model considered in this Letter. Consistent with trivial weak topological indices, STS measurements revealed that full step edges are gapped [53]; partial step edges were not studied. We predict that a partial step edge in Bi₁₃Pt₃I₇ hosts a gapless helical mode.

Helical modes on dislocations can also be measured by their effect on conductivity [9,10].

Discussion.—Our work is a first step in the analysis of partial lattice defects in topological phases. Partial dislocations fall outside the scope of Eq. (1). Nonetheless, we have shown that when a partial Burgers vector can be continuously deformed to a lattice vector by restoring a translation symmetry, the partial dislocation becomes a full dislocation that can host a gapless helical mode subject to the constraint of Eq. (1). We have shown that helical modes on partial dislocation lines can be used to experimentally detect HOTIs since they provide a sufficient condition for higher order topology. Furthermore, in every HOTI it is possible to construct a defect with a gapless helical mode.

There are many possible future directions. The analysis will generalize beyond class AII. Furthermore, a bulk invariant that captures both the intrinsic and extrinsic HOTI models remains an open question; recent progress has been made in Ref. [63]. We show in Supplemental Material, Sec. C [45] that the low-energy theory of the stacking fault can be regarded as an embedded 2D topological insulator. Hence, the entanglement diagnosis in Ref. [46] could potentially identify partial lattice defects that host topological modes in more general models.

*raquel.queiroz@weizmann.ac.il

†i.c.fulga@ifw-dresden.de

‡jennifer.cano@stonybrook.edu

- [1] L. Fu and C. L. Kane, *Phys. Rev. B* **76**, 045302 (2007).
- [2] J. E. Moore and L. Balents, *Phys. Rev. B* **75**, 121306 (2007).
- [3] R. Roy, *Phys. Rev. B* **79**, 195322 (2009).
- [4] Y. Ran, Y. Zhang, and A. Vishwanath, *Nat. Phys.* **5**, 298 (2009).
- [5] J. C. Y. Teo and C. L. Kane, *Phys. Rev. B* **82**, 115120 (2010).
- [6] J. C. Teo and T. L. Hughes, *Annu. Rev. Condens. Matter Phys.* **8**, 211 (2017).
- [7] Z. Ringel, Y. E. Kraus, and A. Stern, *Phys. Rev. B* **86**, 045102 (2012).
- [8] O. A. Tretiakov, A. Abanov, S. Murakami, and J. Sinova, *Appl. Phys. Lett.* **97**, 073108 (2010).
- [9] B. Sbierski, M. Schneider, and P. W. Brouwer, *Phys. Rev. B* **93**, 161105 (2016).
- [10] H. Hamasaki, Y. Tokumoto, and K. Edagawa, *Appl. Phys. Lett.* **110**, 092105 (2017).
- [11] V. Juričić, A. Mesaros, R.-J. Slager, and J. Zaanen, *Phys. Rev. Lett.* **108**, 106403 (2012).
- [12] D. Asahi and N. Nagaosa, *Phys. Rev. B* **86**, 100504 (2012).
- [13] A. Rüegg and C. Lin, *Phys. Rev. Lett.* **110**, 046401 (2013).
- [14] T. L. Hughes, H. Yao, and X.-L. Qi, *Phys. Rev. B* **90**, 235123 (2014).
- [15] F. de Juan, A. Rüegg, and D.-H. Lee, *Phys. Rev. B* **89**, 161117 (2014).
- [16] J. C. Y. Teo and T. L. Hughes, *Phys. Rev. Lett.* **111**, 047006 (2013).
- [17] K. Shiozaki and M. Sato, *Phys. Rev. B* **90**, 165114 (2014).
- [18] R.-J. Slager, A. Mesaros, V. Juričić, and J. Zaanen, *Phys. Rev. B* **90**, 241403 (2014).
- [19] W. A. Benalcazar, J. C. Y. Teo, and T. L. Hughes, *Phys. Rev. B* **89**, 224503 (2014).
- [20] B. Bradlyn, L. Elcoro, J. Cano, M. Vergniory, Z. Wang, C. Felser, M. Aroyo, and B. A. Bernevig, *Nature (London)* **547**, 298 (2017).
- [21] J. Cano, B. Bradlyn, Z. Wang, L. Elcoro, M. G. Vergniory, C. Felser, M. I. Aroyo, and B. A. Bernevig, *Phys. Rev. B* **97**, 035139 (2018).
- [22] B. J. Wieder, B. Bradlyn, Z. Wang, J. Cano, Y. Kim, H.-S. D. Kim, A. M. Rappe, C. L. Kane, and B. A. Bernevig, *Science* **361**, 246 (2018).
- [23] W. A. Benalcazar, B. A. Bernevig, and T. L. Hughes, *Science* **357**, 61 (2017).
- [24] F. Schindler, A. M. Cook, M. G. Vergniory, Z. Wang, S. S. P. Parkin, B. A. Bernevig, and T. Neupert, *Sci. Adv.* **4**, eaat0346 (2018).
- [25] Z. Song, Z. Fang, and C. Fang, *Phys. Rev. Lett.* **119**, 246402 (2017).
- [26] J. Langbehn, Y. Peng, L. Trifunovic, F. Von Oppen, and P. W. Brouwer, *Phys. Rev. Lett.* **119**, 246401 (2017).
- [27] W. A. Benalcazar, B. A. Bernevig, and T. L. Hughes, *Phys. Rev. B* **96**, 245115 (2017).
- [28] M. Geier, L. Trifunovic, M. Hoskam, and P. W. Brouwer, *Phys. Rev. B* **97**, 205135 (2018).
- [29] L. Trifunovic and P. Brouwer, *Phys. Rev. X* **9**, 011012 (2019).
- [30] F. Schindler, Z. Wang, M. G. Vergniory, A. M. Cook, A. Murani, S. Sengupta, A. Y. Kasumov, R. Deblock, S. Jeon, I. Drozdov, H. Bouchiat, S. Guéron, A. Yazdani, B. A. Bernevig, and T. Neupert, *Nat. Phys.* **14**, 918 (2018).
- [31] E. Khalaf, H. C. Po, A. Vishwanath, and H. Watanabe, *Phys. Rev. X* **8**, 031070 (2018).
- [32] E. Khalaf, *Phys. Rev. B* **97**, 205136 (2018).
- [33] M. Ezawa, *Phys. Rev. B* **98**, 045125 (2018).
- [34] M. Ezawa, *Phys. Rev. Lett.* **120**, 026801 (2018).
- [35] A. Matsugatani and H. Watanabe, *Phys. Rev. B* **98**, 205129 (2018).
- [36] S. Imhof, C. Berger, F. Bayer, J. Brehm, L. W. Molenkamp, T. Kiessling, F. Schindler, C. H. Lee, M. Greiter, T. Neupert, and R. Thomale, *Nat. Phys.* **14**, 925 (2018).
- [37] C. W. Peterson, W. A. Benalcazar, T. L. Hughes, and G. Bahl, *Nature (London)* **555**, 346 (2018).
- [38] M. Serra-Garcia, V. Peri, R. Süsstrunk, O. R. Bilal, T. Larsen, L. G. Villanueva, and S. D. Huber, *Nature (London)* **555**, 342 (2018).
- [39] J. Noh, W. A. Benalcazar, S. Huang, M. J. Collins, K. P. Chen, T. L. Hughes, and M. C. Rechtsman, *Nat. Photonics* **12**, 408 (2018).
- [40] Y. You, T. Devakul, F. J. Burnell, and T. Neupert, *Phys. Rev. B* **98**, 235102 (2018).
- [41] L. Fu, *Phys. Rev. Lett.* **106**, 106802 (2011).
- [42] T. H. Hsieh, H. Lin, J. Liu, W. Duan, A. Bansil, and L. Fu, *Nat. Commun.* **3**, 982 (2012).
- [43] A. Altland and M. R. Zirnbauer, *Phys. Rev. B* **55**, 1142 (1997).
- [44] D. Hull and D. Bacon, *Introduction to Dislocations*, 5th ed. (Elsevier, Oxford, 2011).
- [45] See Supplemental Material at <http://link.aps.org/supplemental/10.1103/PhysRevLett.123.266802> for a look-up table for Eq. (2); the correspondence between edge, screw, and hinge modes; a low-energy theory of the stacking fault; a dislocation band structure; and an edge dislocation model; which includes Refs. [4,28,31,46–48].
- [46] T. I. Tügel, V. Chua, and T. L. Hughes, *Phys. Rev. B* **100**, 115126 (2019).
- [47] R. Jackiw and C. Rebbi, *Phys. Rev. D* **13**, 3398 (1976).
- [48] R. Queiroz and A. Stern, *Phys. Rev. Lett.* **123**, 036802 (2019).
- [49] W. P. W. Su, J. R. Schrieffer, and A. J. Heeger, *Phys. Rev. Lett.* **42**, 1698 (1979).
- [50] H. C. Po, A. Vishwanath, and H. Watanabe, *Nat. Commun.* **8**, 50 (2017).
- [51] C. W. Groth, M. Wimmer, A. R. Akhmerov, and X. Waintal, *New J. Phys.* **16**, 063065 (2014).

- [52] I. K. Drozdov, A. Alexandradinata, S. Jeon, S. Nadj-Perge, H. Ji, R. J. Cava, B. Andrei Bernevig, A. Yazdani, B. A. Bernevig, and A. Yazdani, *Nat. Phys.* **10**, 664 (2014).
- [53] C. Pauly, B. Rasche, K. Koepf, M. Liebmann, M. Pratzner, M. Richter, J. Kellner, M. Eschbach, B. Kaufmann, L. Plucinski, C. M. Schneider, M. Ruck, J. van den Brink, and M. Morgenstern, *Nat. Phys.* **11**, 338 (2015).
- [54] P. Sessi, D. Di Sante, A. Szczerbakow, F. Glott, S. Wilfert, H. Schmidt, T. Bathon, P. Dziawa, M. Greiter, T. Neupert, G. Sangiovanni, T. Story, R. Thomale, and M. Bode, *Science* **354**, 1269 (2016).
- [55] R. Wu, J.-Z. Ma, S.-M. Nie, L.-X. Zhao, X. Huang, J.-X. Yin, B.-B. Fu, P. Richard, G.-F. Chen, Z. Fang, X. Dai, H.-M. Weng, T. Qian, H. Ding, and S. H. Pan, *Phys. Rev. X* **6**, 021017 (2016).
- [56] X.-B. Li, W.-K. Huang, Y.-Y. Lv, K.-W. Zhang, C.-L. Yang, B.-B. Zhang, Y. B. Chen, S.-H. Yao, J. Zhou, M.-H. Lu, L. Sheng, S.-C. Li, J.-F. Jia, Q.-K. Xue, Y.-F. Chen, and D.-Y. Xing, *Phys. Rev. Lett.* **116**, 176803 (2016).
- [57] N. I. Fedotov and S. V. Zaitsev-Zotov, *Phys. Rev. B* **95**, 155403 (2017).
- [58] L. Peng, Y. Yuan, G. Li, X. Yang, J.-J. Xian, C.-J. Yi, Y.-G. Shi, and Y.-S. Fu, *Nat. Commun.* **8**, 659 (2017).
- [59] Z.-Y. Jia, Y.-H. Song, X.-B. Li, K. Ran, P. Lu, H.-J. Zheng, X.-Y. Zhu, Z.-Q. Shi, J. Sun, J. Wen, D. Xing, and S.-C. Li, *Phys. Rev. B* **96**, 041108 (2017).
- [60] D. Iaiya, C.-Y. Wang, Y. Maximenko, D. Walkup, R. Sankar, F. Chou, Y.-M. Lu, and V. Madhavan, *Phys. Rev. B* **99**, 155116 (2019).
- [61] Y.-C. Yam, S. Fang, P. Chen, Y. He, A. Soumyanarayanan, M. Hamidian, D. Gardner, Y. Lee, M. Franz, B. I. Halperin, E. Kaxiras, and J. E. Hoffman, [arXiv:1810.13390](https://arxiv.org/abs/1810.13390).
- [62] Z. Wang, B. J. Wieder, J. Li, B. Yan, and B. A. Bernevig, *Phys. Rev. Lett.* **123**, 186401 (2019).
- [63] E. Khalaf, W. A. Benalcazar, T. L. Hughes, and R. Queiroz, [arXiv:1908.00011](https://arxiv.org/abs/1908.00011).